Electronic Supplementary Information

Single-molecule FRET combined with electrokinetic trapping reveals real-time enzyme kinetics of individual ATP synthases

Hendrik Sielaff,[a] Frank Dienerowitz[b] and Maria Dienerowitz*[†c]

[a]*Department of Chemistry, Centre for BioImaging Sciences, National University of Singapore, 14 Science Drive 4, 117557 Singapore, Singapore.*

[b]*Ernst-Abbe-Hochschule Jena, University of Applied Sciences, Carl-Zeiss-Promenade 2, 07745 Jena, Germany.*

[c]*Single-Molecule Microscopy Group, Universitätsklinikum Jena, Nonnenplan 2-4, 07743 Jena, Germany. Email: maria.dienerowitz@york.ac.uk*

* Corresponding author

† Present address: Department of Physics, University of York, Heslington, YO10 5DD, York, UK.

F_OF_1-ATP synthase purification, fluorescent labelling and reconstitution into liposomes

F_OF_1-ATP synthase from *E. coli* carrying an exposed cysteine at the C-terminus of the **a**-subunit (F_OF_1-**a**-GAACA) was expressed and purified according to existing protocols.[1] In brief, the ATP synthase was solubilized from *E. coli* membranes by n-dodecyl-β-D-maltoside and concentrated via a two-step ammonium sulfate precipitation. The resolved precipitate was desalted and delipidated using a Sephacryl S300 column (GE-Healthcare, USA) and further purified by a Poros HQ 20 (4.6 x 100 mm) anion exchange column (Applied Biosystems, USA). Finally, the protein was desalted by size exclusion chromatography using a Tricorn Superose 6 10/300 GL column (GE Healthcare, USA).

The F_1 part harboring an exposed cysteine at position 56 of the ε-subunit was separately expressed and purified. Cytoplasmic membranes were isolated, washed and the F_1 part stripped off. Subsequently, the F_1 part was further purified using a Poros HQ 20 (10 x 200 mm) anion exchange column (Applied Biosystems, USA) followed by a final Tricorn Superdex 200 10/300 GL column (GE Healthcare, USA).

The cysteine at the C-terminus of subunit **a** (F_OF_1) was labelled with AlexaFluor 488 C_5-maleimide and the cysteine in the ε-subunit (F_1) was labelled with ATTO594 maleimide (ATTOtec, Germany). Briefly, the proteins were precipitated with ammonium sulfate, resuspended in 50 mM MOPS-NaOH pH 7.0, 0.1 mM $MgCl_2$ and, in the case of F_OF_1, 0.1% DDM and desalted via a self-packed Sephadex G50 (GE Healthcare) column. Protein concentrations were determined photometrically using a molar extinction coefficient at 280 nm of 310,120 $M^{-1}\cdot cm^{-1}$ for F_OF_1 and 206,060 $M^{-1}\cdot cm^{-1}$ for F_1. Labeling was carried out with a molar protein to dye ratio of 1:1.1 and a protein concentration of 8.7 µM for F_OF_1 and 14 µM for F_1. The reaction was stopped by separating the free dye from the F_OF_1 after 15 minutes and from the F_1 after 8 minutes. Labelling efficiencies were determined photometrically by comparing absorptions using the molar extinction coefficients of the proteins (see above) and the fluorescent dyes, i.e. 72,000 $M^{-1}\cdot cm^{-1}$ for AlexaFluor 488 at 493 nm and of 120,000 $M^{-1}\cdot cm^{-1}$ for ATTO594 at 603 nm. The labelling efficiencies were 63% for F_OF_1 and 40% for F_1. Labelling specificities were over 95%, estimated by 12% SDS-PAGE with subsequent fluorography.

To obtain a double-labelled ATP synthase, F_OF_1-**a**-AlexaFluor 488 was first reconstituted into preformed liposomes[2] resulting in 1.2 ml of 20 nM reconstituted F_OF_1, which corresponds to a protein to liposome ratio of 1:4. Then, F_1 was stripped off under low ionic conditions and labelled F_1 was rebound to the F_O liposomes. The final concentration of F_OF_1 after stripping and rebinding was about 20 nM in 20 mM tricine-NaOH pH 8, 20 mM succinate, 50 mM NaCl, 0.6 mM KCl, 2.5 mM $MgCl_2$ and 10% (v/v) glycerol.

The hydrolysis activities of the two preparations before and after labelling were measured as triplicates via a coupled enzymatic assay.[3] Activities were measured at 21 °C; the same temperature as in the single molecule measurements. Labelling of F_OF_1 at the **a**-subunit and F_1 at the ε-subunit did not have any large effect on the hydrolysis activities (F_OF_1: 12.2 ± 0.9 s^{-1}, F_OF_1-**a**-AlexaFluor 488: 16.4 ± 0.3 s^{-1}, F_1: 29.2 ± 2.4 s^{-1}, F_1-ε-ATTO594: 25.8 ± 1.5 s^{-1}). Furthermore, the labelling did not influence the autoinhibition by the ε-subunit as shown by the high activation with N,N-dimethyl-n-dodecylamine N-oxide (F_OF_1: 12.7 ± 0.9 s^{-1}, F_OF_1-**a**-AlexaFluor 488: 11.4 ± 1.1 s^{-1}, F_1: 7.7 ± 0.7 s^{-1}, F_1-ε-ATTO594: 8.0 ± 0.6 s^{-1}).

We stored the so prepared proteoliposomes at -80 °C in a tricine-succinat buffer (20 mM tricine-NaOH (pH 8.0), 20 mM succinate, 0.6 mM KCl, 50 mM NaCl and 2.5 mM $MgCl_2$). Prior to all experiments, we rapidly defrosted the proteoliposomes to room temperature, diluted them further to 40 pM in a 1:1 mixed solution of deionized water with liposome buffer (20 mM tricine-NaOH pH 8, 20 mM succinate, 0.6 mM KCl, 2.5 mM $MgCl_2$). To this we added the required ATP concentration just before the start of the measurements.

ABEL trap optical setup and instrumentation

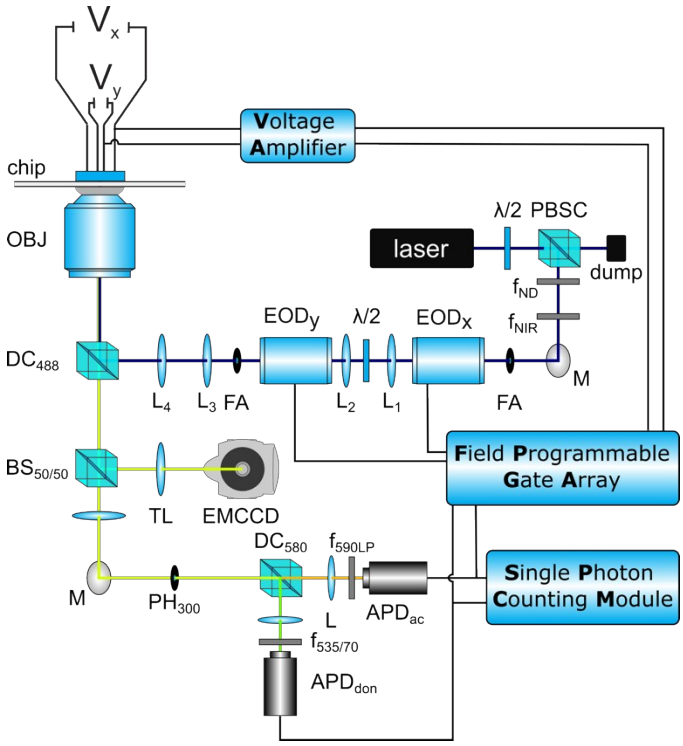

Supplementary Figure 1. Diagram of the optical setup. The laser beam passes half-wave plates (λ/2), a polarising beam splitter cube (PBSC), a neutral density (f_{ND}) as well as an IR filter (f_{NIR}). Lenses L_1 and L_2 image the plane of the first optical deflector EOD_x onto the second EOD_y. Field apertures (FA) block multiple reflections in the system and serve as alignment aids. Dichroic beam splitters DC_{488} and DC_{580} separate the excitation laser from the fluorescent signal as well as the donor from the acceptor signal, respectively. A longpass filter f_{590LP} and a bandpass filter $f_{535/70}$ further discriminate between the acceptor and donor signal. Avalanche photo diodes (APD), mirrors (M), lenses (L), objective (OBJ), pinhole (PH), tube lens (TL) and an optional 50/50 beamsplitter ($BS_{50/50}$) with EMCCD camera complete the setup.

All smFRET ABEL trap experiments were conducted on a purpose-built confocal microscope system[4]. A cw 491 nm laser (Calypso, Cobold, Sweden), attenuated to 40 µW and matched to the excitation spectrum of the AlexaFluor 488 donor fluorophore, facilitates fluorescence detection and FRET to the ATTO594 acceptor fluorophore. We optimized the laser power during preliminary measurements to be high enough to provide sufficient signal over noise but also low enough to avoid premature bleaching of the donor fluorophore. Too high laser powers reduce the achievable trap duration. Two electro-optical beam deflectors (EOD, M310A, Conoptics, USA) situated in the Fourier plane of the trap site introduced an angular deflection to the excitation laser resulting in lateral displacement of the beam along the x and y direction inside the sample plane. The laser traced a 19-point hexagonal scan pattern at f_{scan}=20 kHz.

A piezo-driven stage (P-527.3CD, Physik Instrumente, Germany) incorporated into the microscope (IX71, Olympus) held the sample chamber (PDMS microfluidic chip). The excitation and detection beam path both passed through an oil immersion (n = 1.516, Merck KGaA, Germany) objective (60x, PlanApo N, oil, NA 1.42, Olympus, Germany). To align the sample chamber with the optical beam path prior to a measurement we inserted a 50/50 beamsplitter to view the trapping area and laser spot position with an EMCCD camera (iXonEM+ DU-897, Andor Technology, UK) located at a microscope sideport. A double bandpass dichroic mirror (dualband 488/561rpc, AHF, Germany) separated the detected fluorescence from the excitation laser. A pinhole (300 µm) in the image plane of the tube lens optimized the detection signal-to-noise ratio. A dichroic beam

splitter (HC BS 580 imaging, AHF) spectrally separated the donor and acceptor fluorescence signal before two avalanche photodiodes (APD, SPCM-AQRH 14, Excelitas, USA). A bandpass (f535/70, 535/70 ET, AHF, Germany) and a longpass (f595LP, AHF, Germany) filter further determined the precise wavelength detection range for the donor and acceptor channel respectively. A single-photon counting module (SPCM, DPC230, Becker&Hickl, Germany) recorded arriving photons in a time-tagged mode.

A field programmable gate array module (FPGA, 7852R PCIe, 80 MHz operation frequency, National Instruments, USA) operated the high voltage control (7602M, Krohn-Hite Corporation, USA) of the EODs and controlled the feedback voltage amplifier (built in-house, |VPP| = 20 V) to deliver the electric fields counter-acting the molecule's Brownian motion via platinum electrodes. After correlating the detected photon signals to the scanning pattern positions, an implemented Kalman filter estimated the particle trajectory.[5]

Data acquisition

Just before the start of a measurement, we added the desired ATP concentration to the diluted F_OF_1-ATP synthase proteoliposome and filled 10 μl sample solution into a PDMS chip. Diluting the labelled F_OF_1-ATP synthase proteoliposome ensured a rapid succession of trapping events (minimum 1 within 10 s) without multiple complexes entering the trap site and prematurely aborting the trapping. Data acquisition took on average 1 h measurement time per ATP concentration. We exchanged the active sample mixture every 10-15 min to ensure constant substrate concentrations during the catalytic activity measurements.

During the measurements, every active F_OF_1-ATP synthase hydrolyzed ATP to ADP and P_i. With only 14% molecular motors active and their concentrations in the pM range, we estimated a maximum of 15% ATP molecules consumed by the end of our measurements before we replaced the chip with a fresh sample. This is a maximum estimate assuming three site catalysis for all molecules and every rotation. Based on these low ATP consumption rates we refrained from adding an ATP regenerating enzymatic assay.

Data processing and analysis

The maximum possible time resolution of the single photon counting card (DPC230, Becker&Hickl, Germany) was 165 ps. We applied a 0.1 ms binning (Supplementary Figure 2a) to the raw photon data to both channels – donor and acceptor. We employed a low pass filter to the Fourier transform of the photon time traces in the frequency domain to remove noise (slope of -20 dB / decade). We subsequently transformed the signal back into the time domain as displayed in Supplementary Figure 2b) (black line). A scheme for the data processing workflow is shown in Supplementary Figure 3a. For a uniform data analysis across all different samples, we normalized the so obtained time trace signal according to its maximum and minimum intensity. This circumvented the need to apply varying background reductions to each time trace individually. We set the crossover points between the donor and the acceptor trace as general starting point of a rotation (shown in Supplementary Figure 3b). We refrain from applying a FRET level assignment to our data. All data analysis was performed with self-written software in MATLAB (Mathworks, USA) including embedded C scripts.

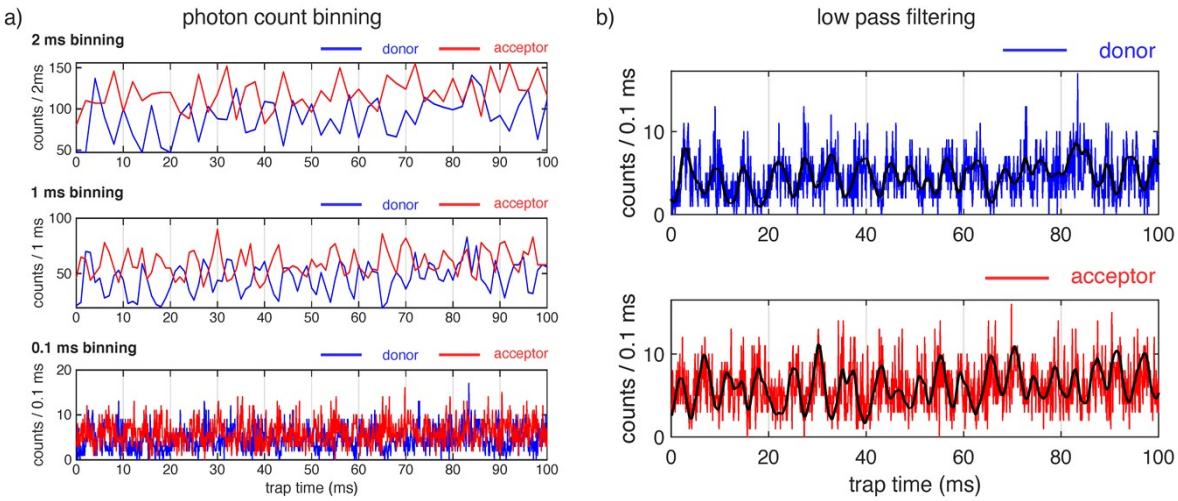

Supplementary Figure 2. Photon count binning compared to low pass filtering. The example chosen here represents the first 100 ms of the trace displayed in the main article in Figure 4b). a) Increasing the length of the time bin leads to loss of details as the two top panels demonstrate. We display both the donor (blue) and acceptor (red) trace in each panel. Alternating donor and acceptor signal indicates a motor rotation. The motor appears to rotate slower when the photon count is binned at 2 ms instead of 1 ms. On the other hand, choosing the time bins shorter (0.1 ms here) results in the rotation information disappearing in the noise of the signal. b) The donor and acceptor photon time traces displayed separately and binned at 0.1 ms. After applying a low pass filter in the Fourier space, the processed photon time traces (black) retain detailed information and reveal the rotation characteristics of the molecular motor.

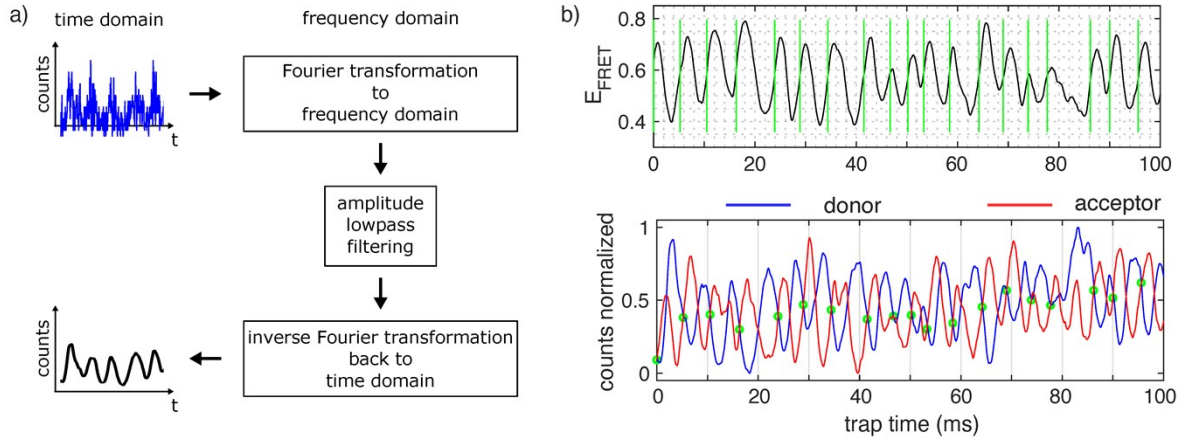

Supplementary Figure 3. Low pass filtering of the raw data and rotation analysis. a) Scheme to describe the data processing, starting with discrete integer values for the time traced photon counts. The low pass filter is applied to the data's Fourier transform within the frequency domain. The time trace data is transformed back to the time domain. b) The bottom panel displays the processed time traced photon counts. The photon counts are normalized for both the donor and acceptor channel individually with respect to their maximum and minimum values to account for different background offsets. The crossover of the donor and acceptor signal at the increase of the acceptor signal (green points) is the starting point of a rotation. The upper panel shows the FRET efficiency with the green lines marking the start of the rotation as determined in the bottom panel (green dots).

Additional data

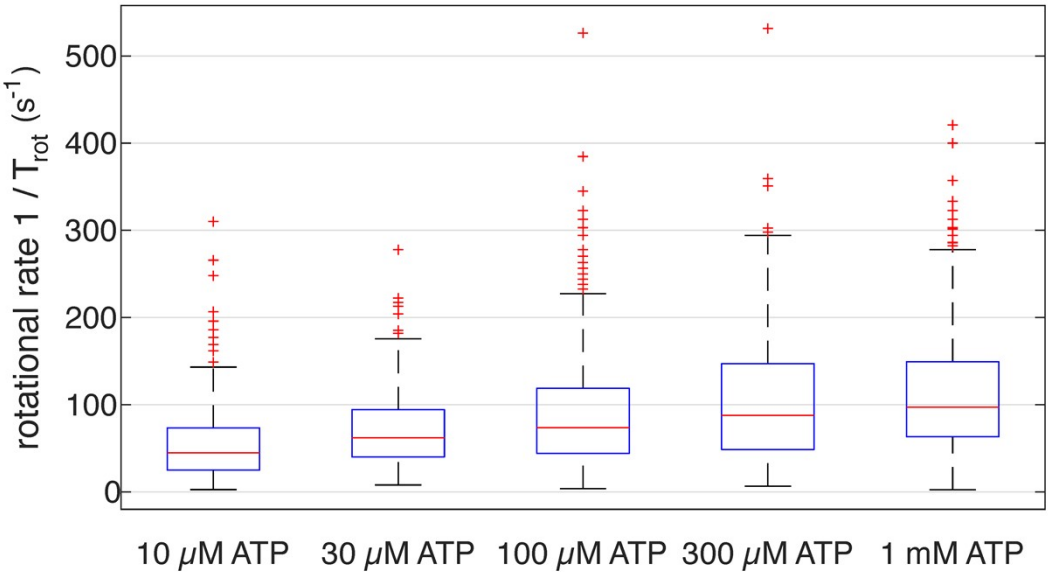

Supplementary Figure 4. The boxplots of rotational rates (1/τ) for different ATP concentrations show the static disorder of the molecules. Figure 5a) in the main text displays the rotation times τ in histogram form. Here, we converted these rotation times into rotational rates.

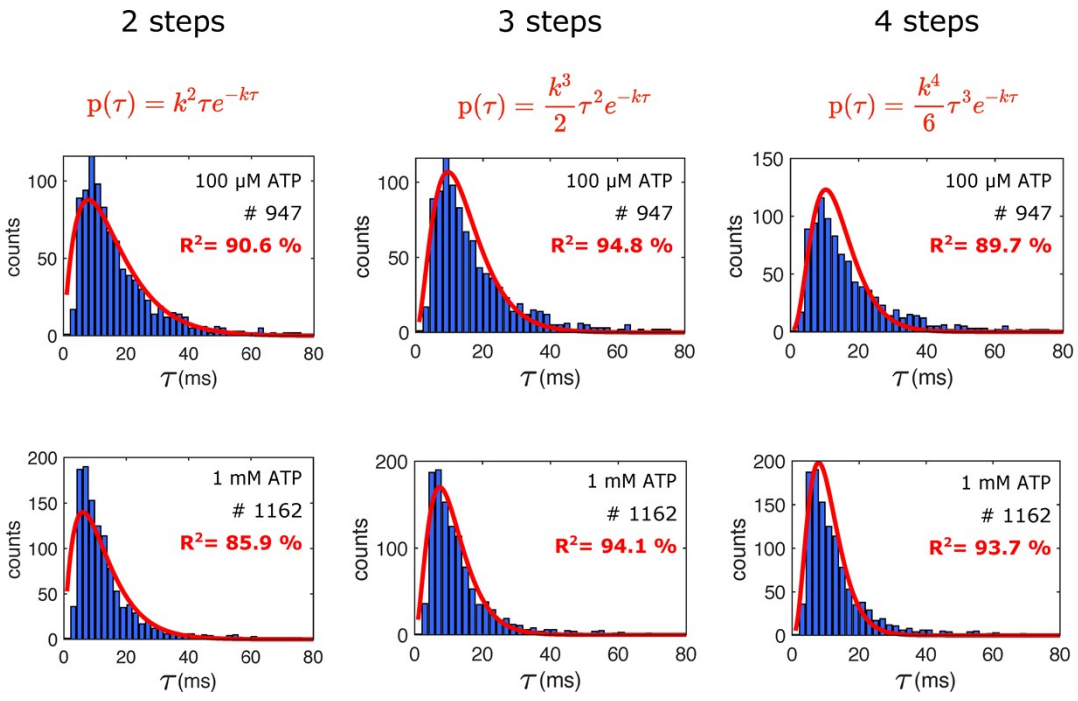

Supplementary Figure 5. Comparison of the 100 μM ATP and 1 mM ATP histogram fits as a function of steps per one full rotation. We fitted the histograms with a gamma distribution (red line) provided in equation 1 in the main article and written above each column. To quantify the goodness of fit we calculated the R^2 value for each fitted histogram. Although we mostly observe only 2 FRET levels during rotation, the best fit (highest R^2) to the histogram data is based on a 3-step rotation as is biologically expected.

Supporting References

1. T. Heitkamp and M. Börsch, *J Phys Chem B*, 2021, **125**, 7638.
2. S. Fischer and P. Gräber, *FEBS Lett.*, 1999, **457**, 327-332.
3. S. Fischer, P. Gräber and P. Turina, *J. Biol. Chem.*, 2000, **275**, 30157-30162.
4. M. Dienerowitz, J. A. Howard, S. D. Quinn, F. Dienerowitz and M. C. Leake, *Methods*, 2021, **193**, 96-106.
5. A. P. Fields and A. E. Cohen, *Proc. Natl. Acad. Sci. U.S.A.*, 2011, **108**, 8937-8942.